Chalcogenide Letters

Tech Science Press

http://doi.org/10.32604/cl.2026.075941

ARTICLE

Photocatalytic Performance of Kaolin/Cu_2CdSnS_4 Composite Synthesized via Solvothermal Route

Hao Guan*, Zicheng Wang, Ruiyang Dai and Tao Dai

School of Materials Science and Engineering, Yancheng Institute of Technology, Yancheng, China
*Corresponding Author: Hao Guan. Email: guanhao1980@sina.com

Received: 11 November 2025; Accepted: 27 January 2026; Published: 28 February 2026

ABSTRACT: Cu_2CdSnS_4 (CCTS) has positioned itself as an efficient option used as a photocatalyst, while kaolin is an ideal catalyst carrier material. In the study, kaolin/Cu_2CdSnS_4 composite catalyst is effectively synthesized by a one-step solvothermal route and applied to remove methylene blue (MB), a typical pollutant in the textile industry. The structural, morphological, and photocatalytic properties of the composite catalyst are characterized by XRD, SEM, FTIR, PL, etc. The results show that a pure kaolin/Cu_2CdSnS_4 composite is obtained. The flower-like structure of Cu_2CdSnS_4 exhibits higher photocatalytic activity due to its relatively large specific surface area, while kaolin creates an ideal carrier. The band gap of the as-obtained kaolin/Cu_2CdSnS_4 composite is estimated to be 1.69 eV. MB's degradation efficiency under simulated solar light irradiation is around 94% within 100 min, with a high rate constant of 0.03 min^{-1}. The recyclability and stability of the composite are investigated. Eventually, the mechanism of photocatalysis was explained. This study depicts that kaolin/Cu_2CdSnS_4 composite is a potential material for effective solar light photocatalytic application.

KEYWORDS: Cu_2CdSnS_4; kaolin; solvothermal; photocatalytic

1 Introduction

Industrial water pollution containing dyes without proper pretreatment has become an ever-increasing challenge, therefore, many new environmentally-friendly technologies in wastewater treatment employing physical, chemical, and biological methods to remove organic contaminants have attracted the interest of many researchers. Among the successful methods, photocatalysis has drawn great attention due to its efficiency, simplicity, and applicability, which can degrade organic contaminants using light energy in the presence of a catalyst. However, the need for UV light for photocatalyst activation limits its practical application due to its low content in solar light; thus, the absorption for improving visible light is enormously important. Many semiconductor materials have been studied as catalysts due to their large absorption range in the visible region. However, traditional photocatalytic materials are hard to simultaneously meet the requirements of broad-spectrum response, high efficiency, durability, and cost-effectiveness for sunlight. Metal sulfides such as In_2S_3, CdS, and PbS have been widely studied as visible-light-driven photocatalysts because of their narrow band gap. As a novel quaternary material, Cu_2ZnSnS_4 (CZTS) has earned special interest among researchers for photocatalysis applications owing to its suitable band gap of around 1.5 eV as well as a large absorption coefficient (>10^4 cm^{-1}) in the visible light region, well carrier transport properties, and adjustable bandgap, etc. [1]. Cu_2CdSnS_4 with a bandgap of 1.4 eV, as well as a large absorption coefficient of 10^5 cm^{-1}, has gotten attention as a proper semiconductor photocatalyst

because of its similar structure to CZTS [2]. To date, Cu_2CdSnS_4 compounds have been prepared by various methods, including solvothermal synthesis, microwave-assisted route, wet chemical technique, successive ionic layer adsorption and reaction technique, thermal decomposition method, and direct liquid coating technology, etc. [3–7]. Meanwhile, Cu_2CdSnS_4 nanoparticles are also researched in the field of photocatalysis and thin film solar cells. However, the aggregation tendency of Cu_2CdSnS_4 nanoparticles may reduce specific surface area and limit adsorption capacity, and conventional synthesis methods are often energy-intensive and environmentally hazardous [8]. These drawbacks have driven recent intensive research into seeking a simple and effective preparation method and powder dispersion process. In order to achieve better dispersion, Kaolin ($Al_2Si_2O_5(OH)_4$) is introduced during the solvothermal synthesis. Kaolin is a common mineral in nature. The unique two-dimensional layer structure makes it have a high surface area and good adsorption capacity, indicating an ideal catalyst carrier material [9–11]. In the last two decades, kaolin has been considered as an ideal carrier for constructing composite catalysts to degrade pollutants under UV/visible light irradiation [12–15]. As far as we know, the study of Cu_2CdSnS_4 loading onto kaolin has not been reported until recently.

In this work, a solvothermal method is adopted to prepare kaolin/Cu_2CdSnS_4 composite. Then, the photocatalytic performance of the obtained kaolin/Cu_2CdSnS_4 composite is investigated by degrading MB as a pollutant model under visible light.

2 Experimental Details

Kaolin ($Al_2Si_2O_5(OH)_4$), $Cu(NO_3)_2{\cdot}3H_2O$, $CdCl_2{\cdot}2.5H_2O$, $SnCl_2{\cdot}2H_2O$ and H_2NCSNH_2 are obtained from Sinopharm Chemical Reagent Co. and are of analytical grade. Based on the previous work, $Al_2Si_2O_5(OH)_4$ (0.1g), $Cu(NO_3)_2{\cdot}3H_2O$ (0.002mol), $CdCl_2{\cdot}2.5H_2O$ (0.001 mol), $SnCl_2{\cdot}2H_2O$ (0.001 mol) and H_2NCSNH_2 (0.006 mol) are dispersed in 80 mL ethylene glycol (EG) under the intensive stirring at room temperature for 2 h, then the solution is transferred into autoclaves and maintained at 200°C for 12 h. The autoclaves are naturally cooled down to room temperature. Finally, the produced samples are collected, washed with deionized water, and dried in vacuum at 80°C for 3 h to obtain the kaolin/Cu_2CdSnS_4 composite.

The phase compositions are measured using X-ray diffraction (X-Pert3 Powder). The surface morphology is observed using scanning electron microscope (Nova Nano SEM 450). The Fourier transform-infrared (FT-IR) spectra are tested by infrared spectrometer (JASCO 3600). The photoluminescence (PL) spectra are analyzed using spectrofluorophotometer (RF-5301 PC). The optical and photodegradation performances are obtained using UV-VIS-NIR spectrometer (UV2450).

3 Results and Discussion

The phase compositions of kaolin, Cu_2CdSnS_4 and kaolin/Cu_2CdSnS_4 samples are acquired using XRD analysis, as shown in Fig. 1. It is noticed that the main reflection peaks at angles of 2θ = 28.1°, 46.9° and 55.8° can be indexed to (112), (220) and (312) crystal planes of Cu_2CdSnS_4 structure, in agreement well with JCPDS 29-0537 card [16]. The average crystallite size estimated from the FWHM of the 28.1° peak using the Debye-Scherrer equation is around 45 nm. Meanwhile, the other diffraction peaks appeared at (2θ) values of 16.4°, 26.2°, 31.2°, 33.2°, 35.4°, 39.3°, 40.8°, 42.6°, 53.6°, 57.5° and 60.8° are well-matched with kaolin structure. All of the diffraction peaks for kaolin and Cu_2CdSnS_4 are present in the XRD pattern of the composite, with no detectable impurities, indicating the successful formation of kaolin/Cu_2CdSnS_4 composite, and the kaolin structure does not change in the reaction process. Simultaneously, we can observe that the diffraction peaks of kaolin/Cu_2CdSnS_4 compared to their pure substances are lower, it is indicated that the crystallinity of kaolin/Cu_2CdSnS_4 composite decreases obviously, revealing a small particle size.

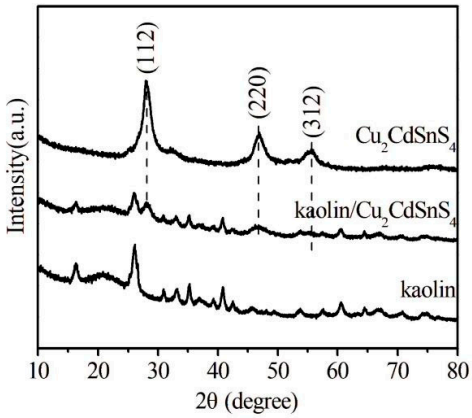

Figure 1: XRD patterns of Cu_2CdSnS_4, kaolin, and kaolin/Cu_2CdSnS_4 samples.

Fig. 2 shows the SEM images of all synthesized samples. Pristine Cu_2CdSnS_4 particles display flower-like hierarchical structures with the peak thickness of about 40–50 nm, in agreement with the result in literature [6]. The kaolin appears as agglomerates of stacked platelets with a thickness of approximately 0.2 μm. Each of these platelets is considered a disposition of several layers, which can supply more adhesion sites for Cu_2CdSnS_4. For kaolin/Cu_2CdSnS_4 composite, after introducing kaolin, the particles of Cu_2CdSnS_4 seem to be distributed on the surface of kaolin. It is indicated that kaolin, as a carrier, effectively inhibits the formation of large-scale aggregates, which is beneficial to photocatalysis.

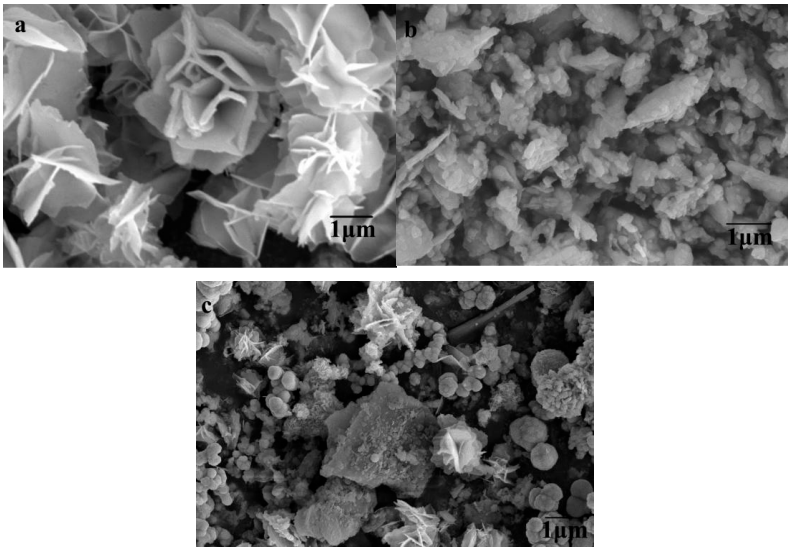

Figure 2: SEM images of (**a**) Cu_2CdSnS_4, (**b**) kaolin, and (**c**) kaolin/Cu_2CdSnS_4 samples.

The FTIR spectra of Cu_2CdSnS_4 and kaolin/Cu_2CdSnS_4 composite is displayed in Fig. 3. The absorption bands occur at 3414 cm^{-1} (characteristic of thiourea or water), 2917 cm^{-1} (S-H thiol functional group or -C=CH- stretching mode), 1632 cm^{-1} (OH bending), 1092 cm^{-1} (metal-thiourea complex), 816 cm^{-1} (C-S stretching or Al-O-Si bond) and 555 cm^{-1} (Al-O-Si bond) [17–19]. Compared to pure Cu_2CdSnS_4, the peak intensity of kaolin/Cu_2CdSnS_4 composite is more apparent, indicating that the prepared composite samples require higher infrared vibration energy, and the internal chemical bonds of Cu_2CdSnS_4 become more stable after dispersion on the surface of kaolin.

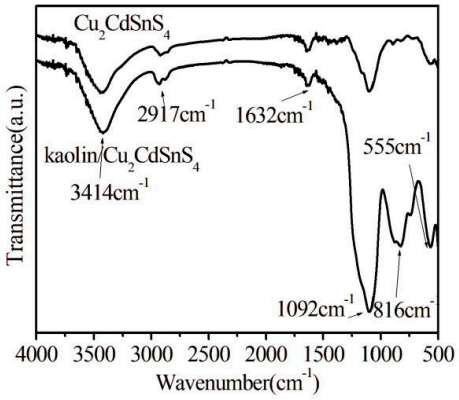

Figure 3: FTIR spectra of Cu_2CdSnS_4 and kaolin/Cu_2CdSnS_4 samples.

It is well known that the photocatalytic properties of many photocatalysts mainly depend on their optical characteristics. The band gap is one of the optical characteristics that can be detected based on Kubelka-Munk theory. The calculated values of all prepared products using Tauc formula by plotting the linear region of $(\alpha h\nu)^2$ vs. $h\nu$ are exhibited in Fig. 4. It can be observed that the band gap of Cu_2CdSnS_4 is estimated at 1.65 eV while the one of the Kaolin is around 3.22 eV, in agreement with those reported in literature [20,21]. For the kaolin/Cu_2CdSnS_4 composite, the band gap is around 1.69 eV, slightly more significant than pure Cu_2CdSnS_4, implying the usage of full spectrum of visible light for good photocatalytic activity.

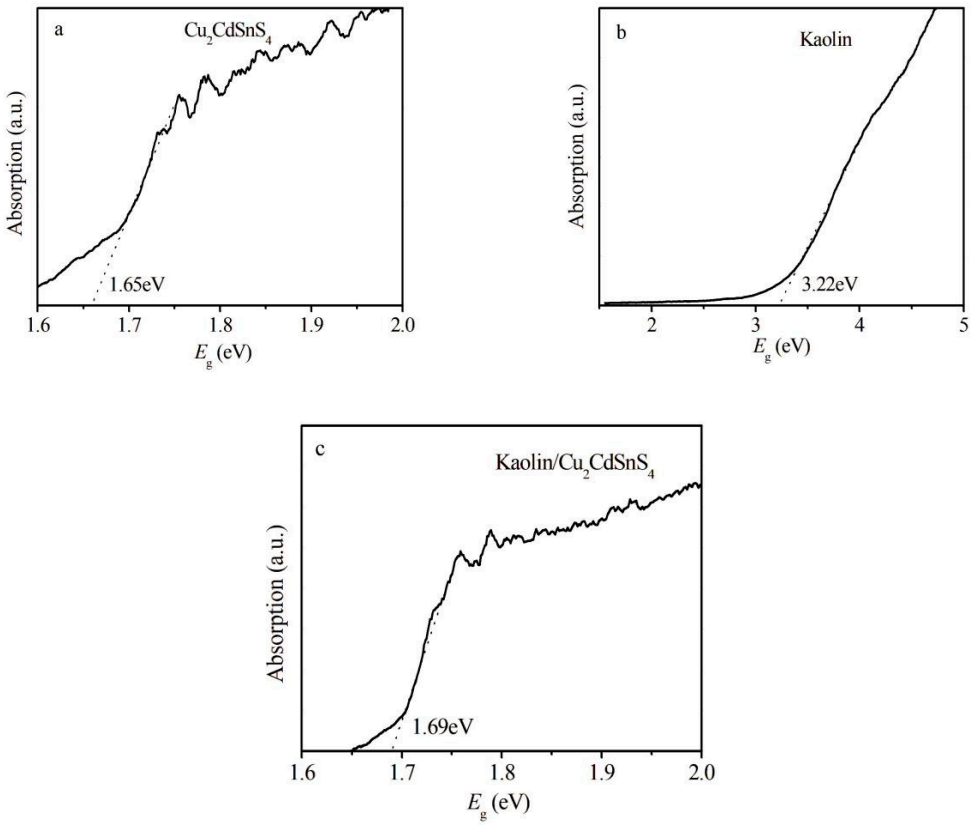

Figure 4: Optical bandgap estimations of (**a**) Cu_2CdSnS_4, (**b**) kaolin and (**c**) kaolin/Cu_2CdSnS_4 samples.

For catalysts, the spatial separation and recombination behavior of photo-induced carriers plays a key role in the photodegradation process. The fluorescence intensity can reflect the probability of recombining photo-induced electrons and holes. Photoluminescence (PL) spectroscopy can be utilized to scrutinize the recombination ability of photogenerated charges. The PL spectra of Cu_2CdSnS_4 and kaolin/Cu_2CdSnS_4 are shown in Fig. 5. The results show that the intensity of PL emission peak of kaolin/Cu_2CdSnS_4 composite is lower reduced compared to pure Cu_2CdSnS_4, indicating that the combination of kaolin/Cu_2CdSnS_4 can effectively inhibit the recombination of electrons and holes. Therefore, Kaolin/Cu_2CdSnS_4 composite is conducive to the transportation and separation of photogenerated electrons-holes, and is expected to exhibit high photocatalytic activity in the visible light.

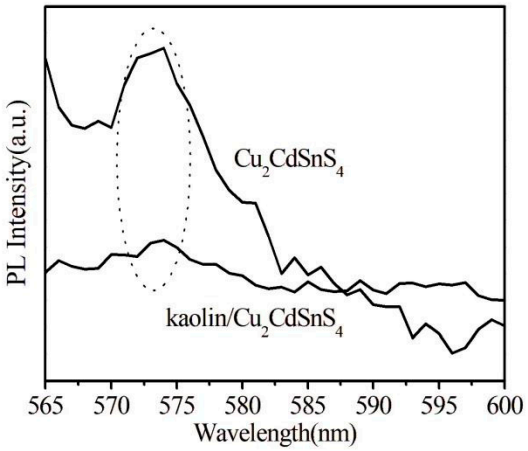

Figure 5: Photoluminescence spectra of Cu_2CdSnS_4 and kaolin/Cu_2CdSnS_4 samples.

The photocatalysis performances of the synthesized products are characterized by degrading methylene blue (MB) as a model for industrial wastewater under the irradiation of visible light for different times. The efficiencies of degradation against the times of light exposure are presented in Fig. 6a. The prepared samples show no significant adsorption for MB in a dark environment for 30 min, implying that MB is a non-biodegradable dye. After 100 min illumination, MB is stable without a photocatalyst and decomposes by only about 2%. When Cu_2CdSnS_4 is added as a catalyst, the MB degradation can increase to 79%. Furthermore, the addition of kaolin/Cu_2CdSnS_4 composite can decompose about 94%, which may be caused by the large surface area as well as the proper band gap value. Compared to other photocatalysts reported in the literature, kaolin/Cu_2CdSnS_4 exhibits higher photocatalytic performance than in previous literature, as shown in Table 1. The result proves that Cu_2CdSnS_4 material opens up a door to visible-light photocatalytic application, and kaolin plays an important role in providing active sites for catalytic Cu_2CdSnS_4. The reaction data are fitted by the pseudo-first-order reaction kinetics model: $\ln(C_0/C) = kt + b$, where k, C_0, and C are the apparent reaction rate constant, MB concentration after adsorption equilibrium and at illumination time t, respectively. As shown in Fig. 6b, the rate constant k is estimated to be 0.01 min^{-1} for Cu_2CdSnS_4 while that of kaolin/Cu_2CdSnS_4 increase to 0.03 min^{-1}. It is clear that kaolin/Cu_2CdSnS_4 composite exhibits the higher reaction rate, inducing the good photocatalytic performance. The cycling performance of kaolin/Cu_2CdSnS_4 composite for the degradation of MB is further examined. It is exhibited in Fig. 6c that the degradation efficiency decreases from 94% to 88% under the identical environments after reuse three times, which may be caused by the reduction of active sites. However, the degradation efficiency is still excellent, indicating reuse stability of kaolin/Cu_2CdSnS_4 photocatalyst. Furthermore, Fig. 6d shows

that the XRD patterns of kaolin/Cu_2CdSnS_4 composite after use has no obviously change compared to that before use, confirming the structural stability, which is in agreement with SEM image of kaolin/Cu_2CdSnS_4 composite after use (Fig. 6e).

Table 1: The similarity of the photocatalytic activity in MB photodegradation from kaolin/Cu_2CdSnS_4 photocatalyst.

Photocatalysts	Degradation Efficiency	Degradation Time	Pollutant	Ref.
Cu_2FeSnS_4	84%	80 min	MB	[22]
Cu_2ZnSnS_4	81.79%	350 min	MB	[23]
$CdIn_2S_4$	84.2%	180 min	MB	[24]
CdS@CuS	95%	240 min	MB	[25]
$Zn_{0.6}Cd_{0.4}S$	63%	80 min	MB	[26]
$AgBiS_2$/UiO-66	90.77%	180 min	MB	[27]
ZnS–$AgInS_2$	>99%	300 min	MB	[28]
kaolin/Cu_2CdSnS_4	94%	100 min	MB	This work

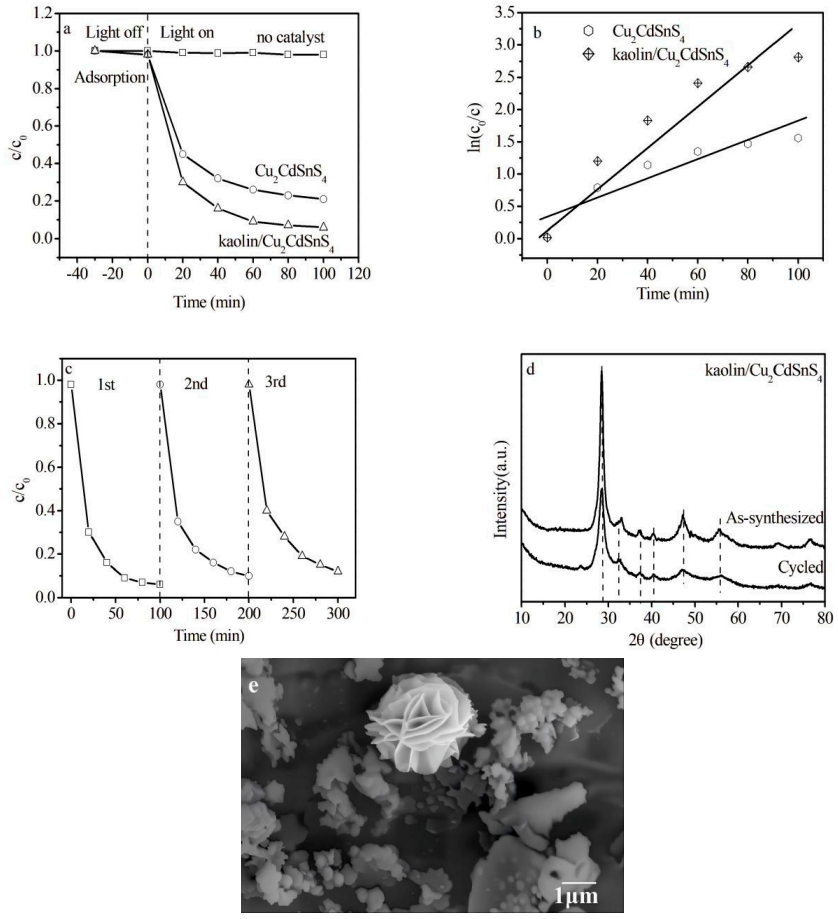

Figure 6: (**a**) the efficiencies of degradation of MB as a function of different time (**b**) ln(c_0/c) as a function of different time of Cu_2CdSnS_4 and kaolin/Cu_2CdSnS_4 composite (**c**) the photo stability of kaolin/Cu_2CdSnS_4 composite (**d**) the structural stability of kaolin/Cu_2CdSnS_4 composite (**e**) SEM image of kaolin/Cu_2CdSnS_4 composite after cycling.

A possible schematic mechanism is shown in Fig. 7. When Uv-Vis irradiation is introduced over CCTS nanoparticles, generation of h^+-e^- takes place. Then these charge carriers migrate on the surface of CCTS nanoparticles, where a redox reaction takes place with other species which are present on the CCTS surface.

h^+ reacts with H2O or OH easily to produce •OH radical. In addition, e^- reacts with O2 to produce $•O_2^-$ radical, and •OH can be obtained further. The produced •OH can oxidize degradation the contaminant due to its high oxidizing potential.

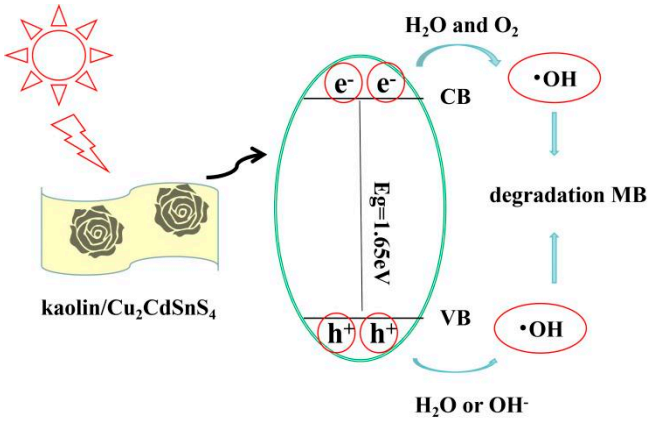

Figure 7: Illustration of photocatalytic redox reaction occurring via photocatalysis to produce •OH to react with MB dye.

4 Conclusion

In this experiment, kaolin/Cu_2CdSnS_4 composite is effectively synthesized using a one-step solvothermal route. It can be seen that Cu_2CdSnS_4 particles exhibit a flower-like hierarchical structure, and the peak thickness is about 40–50 nm. The optical bandgap of the kaolin/Cu_2CdSnS_4 composite is around 1.69 eV, providing a large absorption range in the visible region. Compared to pure Cu_2CdSnS_4, kaolin/Cu_2CdSnS_4 composite exhibits amazing photocatalytic activities for photodegradation of MB of 94% within 100 min irradiation. After repeated use for three cycles, the photodegradation efficiency only decreases to 88%, proving good stability. The work provides a simple and effective method to prepare kaolin/Cu_2CdSnS_4 composite towards photocatalytic applications.

Acknowledgement: Not applicable.

Funding Statement: This work was supported by ongoing funding of Yancheng Institute of Technology. No additional grants to carry out or direct this particular research were obtained.

Author Contributions: Study conception and design: Hao Guan; data collection: Zicheng Wang and Ruiyang Dai; analysis and interpretation of results: Hao Guan and Tao Dai; draft manuscript preparation: Hao Guan and Zicheng Wang. All authors reviewed and approved the final version of the manuscript.

Availability of Data and Materials: Data sharing is not applicable to this article as no datasets were created or analyzed during the current study.

Ethics Approval: Not applicable.

Conflicts of Interest: The authors declare no conflicts of interest.

References

1. Shahzad W, Hassan R, Badawi AK, Ismail B. Novel insights from XRD and photophysical properties of Cu_2ZnSnS_4: Na thin films deposited by aqueous chemical route. J Phys Chem Solids. 2026;208:113116. [CrossRef].
2. Ashebir GY, Dong C. A Cd-diffusion strategy to prepare Cu_2CdSnS_4 thin films for solar cells. Sol Energy Mater Sol Cells. 2026;296:114026. [CrossRef].

3. Ţălu Ş. Morphological study of Cu_2CdSnS_4 nanostructures synthesized *via* spin coating method at different temperatures. Mater Today Commun. 2025;48:113696. [CrossRef].
4. Kamalakannan S, Balasubramaniyan N, Neppolian B. Z-scheme based fabrication of $Cu_2CdSnS4/Au/g\text{-}C_3N_4$ ternary heterojunction with enhanced photocatalytic hydrogen production. Opt Mater. 2025;164:117051. [CrossRef].
5. Vishnupriya S, Choudhari NJ, Kavya DM, Srujana BS, Raviprakash Y. Effect of stacking order on the formation of Cu_2CdSnS_4 thin films synthesized using thermal evaporation technique. J Mater Eng Perform. 2025;34(12):11119–27. [CrossRef].
6. Xu Q, Wang Z, Yang H, Xiang Y, Nie G, Yue W. Synthesis of hierarchical Cu_2CdSnS_4 by microwave-assisted transformation from precursor for photodegradation to malachite green. J Alloys Compd. 2022;904:163966. [CrossRef].
7. Henry J, Prema P, Padiyan DP, Mohanraj K, Sivakumar G. Shape-dependent optoelectrical investigation of $Cu_{2+x}Cd_{1-x}SnS4$ thin films for solar cell applications. New J Chem. 2016;40(3):2609–18. [CrossRef].
8. Yang Y, Waterhouse GIN, Chen Y, Sun-Waterhouse D, Li D. Microbial-enabled green biosynthesis of nanomaterials: current status and future prospects. Biotechnol Adv. 2022;55:107914. [CrossRef].
9. Boonphan S, Prachakiew S, Klinbumrung K, Thongrote C, Klinbumrung A. Enhancing photocatalytic performance of Kaolin clay: an overview of treatment strategies and applications. Arch Environ Prot. 2024;50:54–64. [CrossRef].
10. Liu Z, Zhang Y, Tai Y, Gao R, Liu X, Niu B, et al. Synthesis of $CoFe_2O_4$/natural Kaolin activated peroxymonosulfate for visible light degradation of organic contaminants. Opt Mater. 2022;134:113088. [CrossRef].
11. Awugichew DT, Yu G, Noman M, Jiang R, Yun K, Chen Y. Synthesis and application of Kaolin-based catalyst for the degradation of ciprofloxacin in catalytic ozonation. J Water Process Eng. 2025;70:107070. [CrossRef].
12. Mirbagheri NS, Sabbaghi S. A natural Kaolin/γ-Fe_2O_3 composite as an efficient nano-adsorbent for removal of phenol from aqueous solutions. Microporous Mesoporous Mater. 2018;259:134–41. [CrossRef].
13. Ma W, Hu J, Yoza BA, Wang Q, Zhang X, Li QX, et al. Kaolinite based catalysts for efficient ozonation of recalcitrant organic chemicals in water. Appl Clay Sci. 2019;175:159–68. [CrossRef].
14. Gao L, Zhai Y, Ma H, Wang B. Degradation of cationic dye methylene blue by ozonation assisted with Kaolin. Appl Clay Sci. 2009;46(2):226–9. [CrossRef].
15. Gong Y, Gai L, Tang J, Fu J, Wang Q, Zeng EY. Reduction of Cr(VI) in simulated groundwater by FeS-coated iron magnetic nanoparticles. Sci Total Environ. 2017;595:743–51. [CrossRef].
16. Hao G, Xuye S, Tao G, Lin C. Photocatalytic properties of $Cu_2CdSnS4$-CdS nanocomposites synthesized *via* solvothermal method. Chalcogenide Lett. 2024;21(6):475–82. [CrossRef].
17. Patel M, Mukhopadhyay I, Ray A. Structural, optical and electrical properties of spray-deposited CZTS thin films under a non-equilibrium growth condition. J Phys D Appl Phys. 2012;45(44):445103. [CrossRef].
18. Das K, Panda SK, Gorai S, Mishra P, Chaudhuri S. Effect of Cu/In molar ratio on the microstructural and optical properties of microcrystalline CuInS2 prepared by solvothermal route. Mater Res Bull. 2008;43(10):2742–50. [CrossRef].
19. Gadallah AS, Salim MA, Atwee T, Ghander AM. Effect of Al doping on structural, morphological, optical, and electrical properties of $Cu_2ZnSnS4$ thin films prepared by sol-gel spin coating. Optik. 2018;159:275–82. [CrossRef].
20. Li C, Cao M, Huang J, Wang LJ, Shen Y. Facile synthesis of ultra-long $Cu_2CdSnS4$ nanowires with wurtzite-derived structure. Mater Lett. 2015;140:170–3. [CrossRef].
21. de Freitas VAA, de Souza Pinheiro D, Peixoto CF, de Oliveira LCA, da Costa Couceiro PR. Synthesis of Fe-zeolites from Amazonian kaolinite for methylene blue removal: adsorption and photocatalytic activity. Dalton Trans. 2025;54(20):8287–97. [CrossRef].
22. Abbas A, Li K, Guo X, Wu A, Ali F, Attique S, et al. Solvothermal synthesis of 3D hierarchical Cu_2FeSnS_4 microspheres for photocatalytic degradation of organic pollutants. Environ Res. 2022;205:112539. [CrossRef].
23. Gao Y, Long F, Wang J, Zhang J, Mo S, Zou Z. Understanding the growth mechanism of wurtzite $Cu_2ZnSnS4$ nanocrystals and the photodegradation properties. Mater Des. 2017;123:24–31. [CrossRef].
24. Shi K, Wang Z, Li X, Xiao Q, Ji W, Zhang J, et al. A dual-functional adsorption-photocatalysis system driven by interfacial charge dynamics in a type-II 3D/2D CdIn2S4/nickel metal–organic layer heterojunction for environmental purification and water splitting. J Colloid Interface Sci. 2026;703:139230. [CrossRef].

25. Li J, Weng Q, Huang J, Zou Y. Fabrication of 3D hierarchical CdS@CuS hollow heterostructure nanocages for enhanced visible-light-driven dye degradation. Mater Sci Semicond Process. 2026;202:110178. [CrossRef].
26. Lü Y, Qiao QA, Wang R, Dong Y, Cai H, Gao H. Facile construction of $Zn_{0.6}Cd_{0.4}S/Bi_3O_4Br$ S-scheme heterojunction with enhanced performance under visible light: an experimental and theoretical study. J Environ Chem Eng. 2026;14(1):120748. [CrossRef].
27. Wu Y, Zhang C, Pan Q, Su X, Yi G, Oderinde O. Excellent performance of $AgBiS_2$/UiO-66 Z-scheme heterojunction for amplified CO_2 reduction enhancement and pollutants photodegradation: interface effect and DFT studies. J Photochem Photobiol A Chem. 2026;473:116915. [CrossRef].
28. Maji SK. Single-source derived ZnS–$AgInS_2$ nanocrystals as tuneable dual-function nanoprobes for photocatalytic and bioimaging applications. Inorg Chem Commun. 2026;183:115862. [CrossRef].